# Preparation and Characterization of EVA/Clay Nanocomposites with Improved Barrier Performance

**Runcy Wilson,[1] Tomás S. Plivelic,[2] Abi Santhosh Aprem,[3] C. Ranganathaiagh,[4] S. Anil Kumar,[5] Sabu Thomas[6]**

[1]*School of Chemical Science, Mahatma Gandhi University, P. D Hills P.O, Kottyam, Kerala 686560, India*
[2]*MAX-lab, Lund University, P.O. Box 118, 22100-Lund, Sweden*
[3]*Corporate R&D Division, Hindustan Latex Ltd., Karamana, Trivandrum, Kerala 695002, India*
[4]*Department of Studies in Physics, University of Mysore, Manasagangotri, Mysore, Karnataka, 570006, India*
[5]*Department of Chemistry, N.S.S College, Ottapalam, Palakkad, Kerala, India*
[6]*Centre for Nanoscience and Nanotechnology, Mahatma Gandhi University, P.D Hills P.O, Kottyam, Kerala 686560, India*

Received 12 February 2011; accepted 19 May 2011
DOI 10.1002/app.34966
Published online 30 September 2011 in Wiley Online Library (wileyonlinelibrary.com).

**ABSTRACT:** Poly (ethylene-*co*-vinyl acetate) (EVA)/clay nanocomposites containing two different organoclays with different clay loadings were prepared. The transport of gases (oxygen and nitrogen) through the composite membranes was investigated and the results were compared. These studies revealed that the incorporation of nanoclays in the polymer increased the efficiency of the membranes toward barrier properties. It was also found that the barrier properties of the membranes decreased with clay loadings. This is mainly due to the aggregation of clay at higher loadings. The morphology of the nanocomposites was studied by scanning electron microscopy, transmission electron microscopy and X-ray scattering. Small angle X-ray scattering results showed significant intercalation of the polymer chains between the organo-modified silicate layers in all cases. Better dispersed silicate layer stacking and more homogeneous membranes were obtained for Cloisite® 25A based nanocomposites compared with Cloisite® 20A samples. Microscopic observations (SEM and TEM) were coherent with those results. The dispersion of clay platelets seemed to be maximized for 3 wt % of clay and agglomeration increased with higher clay loading. Wide angle X-ray scattering results showed no significant modifications in the crystalline structure of the EVA matrix because of the presence of the clays. The effect of free volume on the transport behavior was studied using positron annihilation spectroscopy. The permeability results have been correlated with various permeation models. © 2011 Wiley Periodicals, Inc. J Appl Polym Sci 123: 3806–3818, 2012

**Key words:** EVA/organoclay nanocomposites; X-ray scattering (SAXS and WAXS); TEM; free volume; gas transport

## INTRODUCTION

Polymer/clay nanocomposites are two phase systems that consist of a polymeric matrix and dispersed inorganic particles of nanometer sizes. The most common inorganic particles belong to the family of 2 : 1 phyllosilicate clays. Two particular characteristics of layered silicate play an important role in the creation of nanocomposites: the first is the ability of silicate sheets to disperse into individual layers, and second, is the possibility to modify their surface chemistry through ion exchange reactions with organic and inorganic cations.[1] Because of the unique nanometer size dispersion of the layered silicate, nanocomposites exhibit improvement in several properties even at a very low volume fraction loading in the polymer matrix. Polymer/clay nanocomposites present nanostructure morphologies by forming intercalation or exfoliation of individual silicate layer in the polymer matrix. Intercalation entails ordered structures of silicate layers that increase the distance between the adjacent layers because the polymer chain gets into the interlayer spaces. Exfoliation is the process in which the individual silicate layer, originally packed together in an order structure, becomes homogenously dispersed throughout the polymeric matrix.

Polymer/clay nanocomposites have drawn considerable interest because of their enhanced properties, including flame resistance,[2] mechanical properties,[3,4] gas barrier properties,[5–7] thermal stability,[8,9] and biodegradability when compared with pristine polymers. Polymer/clay nanocomposites have also been used in various consumer products and in construction and transportation industry, with specific impact on technologies, such as barrier layer materials, drinks packaging applications, bottle applications, protective coatings and adhesive molding compounds.

*Correspondence to:* S. A. Kumar (anugraha_anil@yahoo.co.in) or S. Thomas (sabuchathukulam@yahoo.co.uk).
Contract grant sponsors: UGC (New Delhi), KSCSTE (Trivandrum), DST.

Poly (ethylene-*co*-vinyl acetate), EVA, is a copolymer of ethylene and vinyl acetate segments, typically formed via free radical polymerization. EVA generally contains 1–50% of the vinyl acetate comonomer along the carbon chain backbone. One of the main advantages of the polymer/clay nanocomposites is their enhanced barrier properties compared with pure polymeric matrix. The impermeable clay layers force a tortuous path way for a permeate transverse the nanocomposites. It was reported that the gas permeability through the polymer films can be reduced with small loadings of nanoclays.[10]

The permeation of plastic films and other packaging materials to gases and vapors is of practical interest. The permeability constants of water vapor, $CO_2$, and oxygen are needed for the design of packing materials. The food packaging industry places particular demands on the barrier properties of their products. The presence of nanoparticles is regarded greatly to reduce the permeability of the pure polymer.[11]

The transport of helium through unmodified and nanoclay modified polyurethane membranes has been studied by Bhowmick and coworkers[12] They found that the well dispersed modified nanoclays contribute to improvement of the permeability properties to a great extent when compared with the aggregated unmodified ones. Adame and Beall[13] showed that the plate like morphology of the clays was the dominant factor in improving barrier properties and they proposed a simple two-dimensional model in which the clay platelets acted as barriers to the gas diffusion thus making the effective path length longer. Poly (dimethyl siloxane-urethane) nanocomposite membranes with various concentrations of polyhedral oligomeric silsesquioxanes were synthesized and the influence of polyhedral oligomeric silsesquioxanes molecules on gas transport properties was studied by Madhavan and Reddy.[14] Khounlavong and Ganesan[15] observed that the addition of impenetrable nanofillers into a rigid polymer matrix resulted in the enhancement of the composite membrane's permeability to gas penetrants and they noted the influence of interfacial layers on transport properties.

The aim of this study is to investigate the gas transport properties of poly (ethylene-*co*-vinyl acetate) (EVA)/clay nanocomposites membranes. The morphology of nanocomposites was analyzed by small angle X-ray scattering (SAXS), scanning electron microscopy (SEM), and transmission electron microscopy analysis (TEM). Positron annihilation life time spectroscopic analysis (PALS) was used to estimate the free volume of nanocomposites. The dielectric loss data was also used to understand the uniformity of the clay dispersion. The thermal stability of the composites was analyzed by thermo gravimetric analysis (TGA). The transport of gases (oxygen and nitrogen) through composite membranes was also investigated. Various theoretical models have been applied to explain the observed permeability of the different nanocomposites.

**TABLE I**
**Descriptive Properties of Nanoclays**

| Nanoclays | Organic modifier used | Modifier concentration |
|---|---|---|
| Cloisite® 20A | Dimethyl, di hydrogenated tallow, quaternary ammonium | 125 meq/100 gm of clay |
| Cloisite® 25A | Dimethyl, hydrogenated tallow, 2-ethylhexyl quaternary ammonium | 95 meq/100 gm of clay |

## EXPERIMENTAL

### Materials

EVA, with 18 mol % vinyl acetate content was obtained from Taisox industries Limited, Taiwan. The crosslinking agent used was dicumyl peroxide (DCP). The nanoclays Cloisite® 20A and Cloisite® 25A were obtained from the Southern Clay Products, United States. The descriptive properties of the nanoclays are cited in Table I

### Membrane fabrication

Organically modified nanoclay-EVA membranes were prepared by melt mixing using dicumyl peroxide as the curing agent. The amount of the DCP used was 2 wt %. The mixing was done in a two roll mixing mill at a nip gap of 1.3 mm and at a friction ratio of 1 : 1.4. The nip gap, mill speed ratio, time of mixing, and temperature of the rolls were kept constant for all mixes. The vulcanization behavior of samples was studied by using Monsanto Rheometer. The sheeted out samples was compression molded in a hydraulic press at 160 C under a load of $24.5 \times 10^4$ N. The samples were prepared with different clay content and designated as $C_3$, $C_5$, $C_7$ for Cloisite® 20A and $D_3$, $D_5$, $D_7$, for Cloisite® 25A. The subscript number represents the amount of grams of nanoclays used per 100 g of the polymer. Pure polymeric EVA membranes were also prepared for comparison.

### Membrane characterization

Small angle X-ray scattering (SAXS)

The SAXS experiments were carried out at I711 beamline of the MAX-lab Synchrotron, Sweden. A monochromatic beam of 1.1 Å wavelength was used and the sample detector distance was 1245.5 mm for

all samples. Two-dimensional pictures were registered using a 2D-CCD detector (165 mm active area, from MAR research, GmbH) with 10 min of data acquisition. Multilayer samples of 1 mm thickness were prepared by stacking pieces cut from a single film. The original orientation of the samples was preserved in the stack. The samples were placed in a multiple position sample holder and measured in an evacuated chamber.

X-ray scattering data were analyzed with the program FIT2D.[16] Average radial intensity profiles, I (q), as a function of the scattering vector $q$ ($q = 4\pi/\lambda \sin(\theta)$, where $2\theta$ is the scattering angle and $\lambda$ is the wavelength) were obtained by integrating the data in the complete image. For the comparison of scattering curves, the intensities were normalized by the integrated intensity incident on the sample during exposure, and corrected by sample absorption, parasitic scattering and background detector.

### Wide angle X-ray scattering (WAXS)

Wide angle X-ray scattering (WAXS) measurements were carried out at the 911-5 beamline of the MAX-lab Synchrotron, Sweden.[17] The wavelength used was 0.907 Å and the sample detector distance was 150.6 mm. Silicon powder was used as a calibration standard for peak positions. Two-dimensional images were recorded using a CCD detector (165 mm active area, from MAR research, GmbH) with 5 minutes of data acquisition. Films of around 15 × 15 mm size and 0.2 mm thickness were placed on the top of a goniometric head with the beam perpendicular to the film surface. Average radial intensity profiles, I ($2\theta$), were obtained integrating the data in the image with the software FIT2D.

### Scanning electron microscopy (SEM)

The surface morphology of the samples was analyzed by SEM imaging. The micrographs of the polymer/clay nanocomposites were taken in JEOL (Japan), Model JSM 6390 electron microscope with an accelerating voltage of 10 kV. The specimens were prepared cryogenically by fracturing the vulcanized sheets in liquid nitrogen and platinum coated to avoid the electro static charge dissipation.

### Transmission electron microscopy (TEM)

The dispersion of layered silicates in polymer nanocomposites was investigated using TEM. The micrographs of the nanocomposites were taken in JEOL JEM transmission electron microscope with an accelerating voltage of 200 keV. Ultrathin sections of bulk specimens (about 100 nm thickness) were obtained at −85°C using an ultra microtome fitted with a diamond knife.

### Positron annihilation life time (PALS)

Positron annihilation spectroscopy is well recognized as a powerful tool for the microstructural investigation of condensed matter. PALS is used to investigate the changes in free volume in the EVA/nanoclay composite membranes. The positron life time spectrometer consists of a fast–fast coincidence system with $BaF_2$ scintillators coupled to photo multiplier tubes type XP2020/Q with quartz window as detectors. The detectors were conical shaped to achieve better time resolution. A 17 μCi$^{22}$ Na positron source deposited on a pure Kapton foil of 0.0127 mm thickness was placed between the two identical pieces of sample under investigation. This sample source sandwich was positioned between the two detectors of PALS to acquire life time spectrum. The spectrometer measures 180 ps as the resolution function with $^{60}$Co source.

However, for better count rate, the spectrometer was operated at 220 ps time resolution. All life time measurements were performed at room temperature and two to three positron life time spectra with more than a million counts under each spectrum were recorded. In PALS analysis mainly two parameters were measured, namely *o*-Ps life time $\tau_3$ and *o*-Ps intensity $I_3$. $\tau_3$ measure the size of free volume holes ($V_f$) and $I_3$ is a relative measure of the number of free volumes sites in the polymer matrix.

### Dielectric measurements

The dielectric loss of the composites was recorded by an Agilent E 4980A LCR meter capable of measuring 20 Hz to 2 MHz. The disc shaped sample of diameter 1.96 cm was dried in a desiccator at reduced pressure and made into a parallel plate capacitor by placing it in between two electrode plate for analysis. All the measurements were done at room temperature.

### Thermo gravimetric analysis (TGA)

Thermo gravimetric analysis of the composites was performed using a TG analyzer DTG-60 to study the systematic weight loss and the thermal stability of specimens. The measurements were carried out between ambient temperature and 800 C at a heating rate of 10 C/min under nitrogen atmosphere with a flow of 100 mL/min.

### Permeability measurements

The LYSSY AG L 100–5000 is used for the determination of the gas permeability of thin films with a

thickness between 0.1 and 2 mm and having permeability range of 0.3–10,000 mL/m$^2$ day, which covers more than 90% of all known thin films. This can be used for precise and reproducible measurements within acceptable measuring times for most of the common gases. The gas permeability was tested according to ASTM D1434 norm. The sample dimensions for the test were: surface area 50 cm$^2$, size 100 × 110 mm and thickness 0.01–5 mm. The measuring interval of the testing was 2.5 mbar-1000 mbar. The time consumption for one sample is at level 1–5 N mL/m$^2$ day 1–5 h and at level 100 N mL/m$^2$ day lower than 1 h. The gas flow rate in both chambers was fixed between 5 and 10 L/h.

## RESULTS AND DISCUSSION

### X-ray scattering analysis (SAXS and WAXS)

Koo et al.[18] reported that the microstructure of silicate layers in polymer/clay nanocomposites evolute through distinct four steps (intercalation, dual states of exfoliation and intercalation, ordered exfoliation, and disordered exfoliation), which are determined by balancing the affinity between polymer and silicate against interactions between silicate platelets such as attractive and steric interactions. At high concentration of silicate, the final morphology is dominated by strong attractive interaction (e.g., Van der Waals interaction) between adjacent silicate layers. This is due to the spatial proximity between layers where Van der Waals interactions are dominant. At intermediate concentration of silicate, the morphology is dominated by the steric interaction rather than attractive force because the interdistance between adjacent silicate layers is too long for them to interact by Van der Waals forces but close enough to interact by steric interaction. At low concentration of silicate, the morphology is not governed by inter-silicate layer interactions because the affinity between the polymer chain and layered silicate overwhelms them.

The X-ray scattering method (SAXS and/or WAXS) has been used to characterize the formation and structure of the polymer-silicate hybrid by monitoring the position, shape, and intensity of the basal reflection from the silicate layers. When the insertion of polymer chains in the silicate layer occurs, an increase of silicate layer volume, and corresponding layer spacing could be obtained, which in turn give rise to the shifting of scattering peaks to lower angles. Scattering peaks cannot be seen in the case of fully exfoliated structures where the silicate layers are completely and uniformly dispersed into a continuous polymer matrix.

The SAXS patterns of neat EVA and nanocomposites (C and D series) are shown in Figure 1(a,b). All SAXS curves including pure EVA sample, present a first peak centered on $q = 0.06$ Å$^{-1}$ (indicated by an arrow in both figures). This feature can be associated to the lamellar periodicity produced in the semi crystalline polymeric matrix and is out of the scope of the present article. On the other hand, at high $q$ values ($q > 0.1$ Å$^{-1}$) two peaks are observed in all curves for nanocomposites (named $d_1$ and $d_2$ for the first and second reflection, respectively). The $d$-spacing of the samples obtained from the *fitted* position of the maximum ($q_m$) and using the relationship $d = 2/q_m$ are summarized in Table II. To fit the experimental data in this $q$ range, the addition of two Lorentzian functions and an exponential baseline was used.

For sample series C [Fig. 1(a)], $d_1$ and $d_2$ values follow the relationship 2 : 1, indicating that they are the first and second order reflection of same structure. Furthermore, as all $d_1$ values are clearly larger than the reported ones for pure organoclay Cloisite® 20A ($d_{mc} = 23.70$ Å from our measurements, 24 Å[19] or 22.4 Å[20] where $d_{mc}$ means the $d$-spacing of the modified clay. See Table II), an intercalated polymer/clay morphology is observed for this series. For those samples, the "$d_2$-peak" is a second order reflection of $d_1$. It means that composites have a very well organized and regularly spaced intercalated structure. No significant changes of the $d$-spacing values are observed for the different clay contents studied.

For sample series D [Fig. 1(b)], the situation is slightly different. $d_1$ is still bigger than the pure modified clay Cloisite® 25A ($d_{mc} = 20.7$ Å from our measurements and also in reference 20, see Table II) indicating an intercalated morphology in the system. However, the $d_2$ values did not satisfy completely a multiple relationship with $d_1$, and also, both peaks shows similar full width half maximum values (FWHM). These facts indicate that $d_1$ and $d_2$ peaks are originated from different periodic structures of the silicate layers. As $d_2$ values are close to $d_{mc}$ for Cloisite® 25A, the second periodic structure can be due to poorly intercalated polymer/clay structures or only unmodified organoclay periodicity.

For completeness the XRD data of pure modified clay powders, Cloisite® 20A and Cloisite® 25A, is shown in Figure 1(c). In each case, the $d$-spacing value obtained from the first peak, $d_{mc}$, is indicated in the figure and listed in Table II. In both cases, a good agreement with previously reported values was obtained.

Finally, from the scattering data, a comparison between the effects of the different organoclays in the nanocomposites can be discussed. The average periodicity of the C series samples (Cloisite® 20A nanocomposites) is higher than D series samples (Cloisite® 25A nanocomposites) by ~ 5 Å, but the

degree of intercalation ($d_1 - d_{mc}$ distance) is quite similar (between 12 and 11 Å in both cases). However, the first peaks of the intercalated structure for Cloisite® 25A nanocomposite series [see Figure 1(a,b)] are less intense and wider (i.e., bigger FWHM) than the $d_1$ peaks of Cloisite® 20A nanocomposite series. This is an indication that the nanoclays dispersions in D series samples are better than in C series samples.

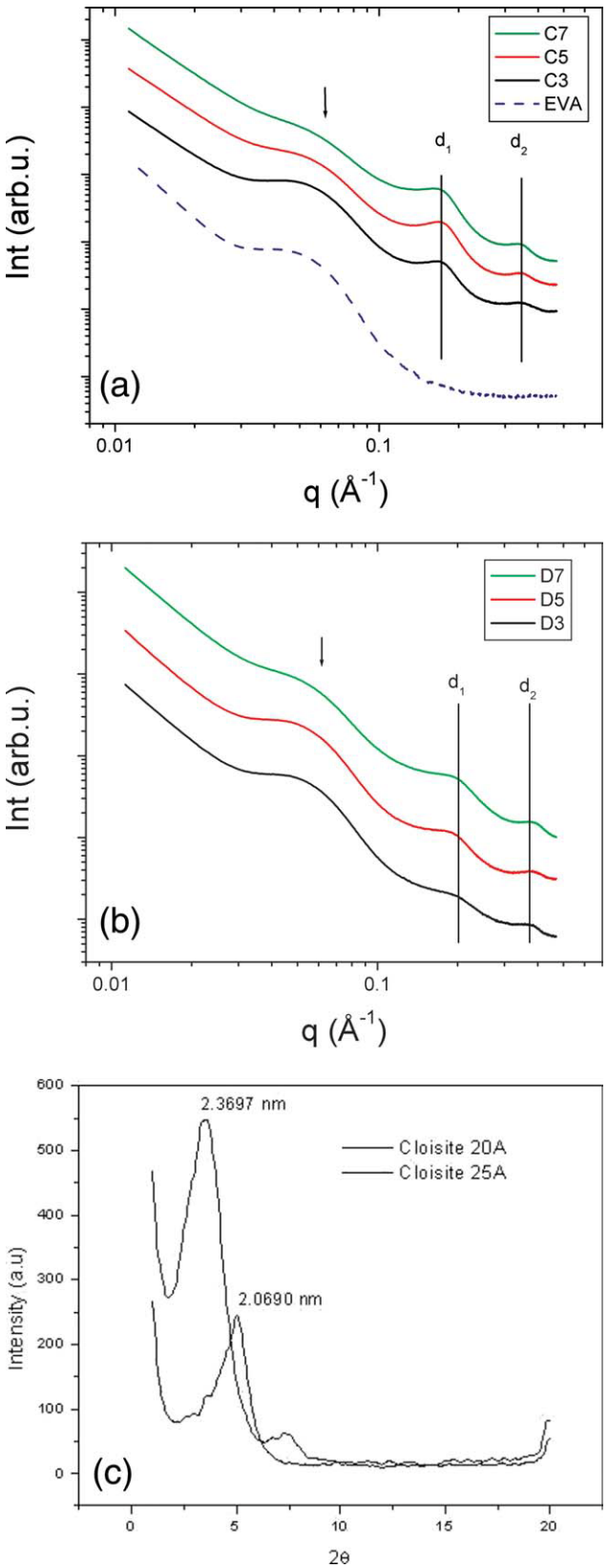


**Figure 1** (a) SAXS curves for EVA/Cloisite® 20A nanocomposites. Solid lines, nanocomposites $C_3$, $C_5$, $C_7$; dotted line, pure polymeric EVA membrane. (b) SAXS curves for EVA/Cloisite® 25A nanocomposites.The curves were multiplied by an arbitrary scale factor to better visualize the sample behavior. The solid line indicates the peak positions with *d*-spacings $d_1$ and $d_2$, for the lowest clay concentration on the samples. The arrows show the peaks associated with the lamellar structure of the semicrystalline polymeric matrix. (c) XRD data for pure modified clay powders Cloisite® 20A and 25A.[Color figure can be viewed in the online issue, which is available at wileyonlinelibrary.com.]

The 2D SAXS images of nanocomposite can be very useful in the understanding of the relative orientation of the silicate layers and their degree of dispersion inside the polymeric matrix. Figure 2(a,b), represent the SAXS data for the highest clay concentration in both series, $C_7$ and $D_7$. For $C_7$ an anisotropic ring is noticeable for the first order reflection of the intercalated polymer/clay stacking period but for the other sample, an almost uniform intensity in the ring was detected. The comparison of the anisotropy can be better observed in Figure 2(c) using an azimuthal representation of the scattered intensity, I (φ) *versus* (where $\varphi = 0$ when the scattering vector is at the equator and $\varphi = 90°$ at the meridian of the image). It is clear that a significant increase in the FWHM of the peaks is observed for sample $D_7$, indicating a more isotropic reflection. Similar results can also be observed from the comparison of the other clay contents. These results probes that the periodic structures of nanocomposites based on Cloisite® 25A organoclay are better dispersed in the film plane than Cloisite® 20A samples series.

The presence of one bulky alkyl tail in Cloisite® 25A (D series nanocomposites) compared to two bulky alkyl tails in Cloisite® 20A (C series samples) leads to better dispersion of nanoplatelets. As the number of bulky groups increases, the level of attraction between the polymer and the organoclay decreases, since the polymer chains have no affinity for the aliphatic tails of the organic modifier. Increasing the number of bulky alkyl tails has two unfavorable effects: First, it limits the number of polymer-silicate contacts by sterically blocking the surface, and second, it increases the amount of alkyl material that would have to mix with the polymer. This reasoning is consistent with the research views proposed by Vaia and Giannelis.[21,22]

The wide angle X-ray scattering data collected for both series C and D bring more details about the

**TABLE II**
**d-spacing Values of Different Nanocomposites and Modified Clays**

| Sample | $d_1$(Å) | $d_2$(Å) | dmc values this work (Å) | Reported $d_{mc}$ values in the literature (Å) |
|---|---|---|---|---|
| $C_3$ | 36.17(2) | 17.97(1) | Cloisite® 20A 23.7(1)Å | Cloisite® 20A 24,[19] 22.4[20] |
| $C_5$ | 35.80(1) | 17.96(1) | | |
| $C_7$ | 36.46(1) | 18.26(1) | | |
| $D_3$ | 31.46(5) | 16.72(1) | Cloisite® 25A 20.7(1) | Cloisite® 25A 20.7[20] |
| $D_5$ | 32.49(2) | 16.33(1) | | |
| $D_7$ | 31.57(1) | 16.12(1) | | |

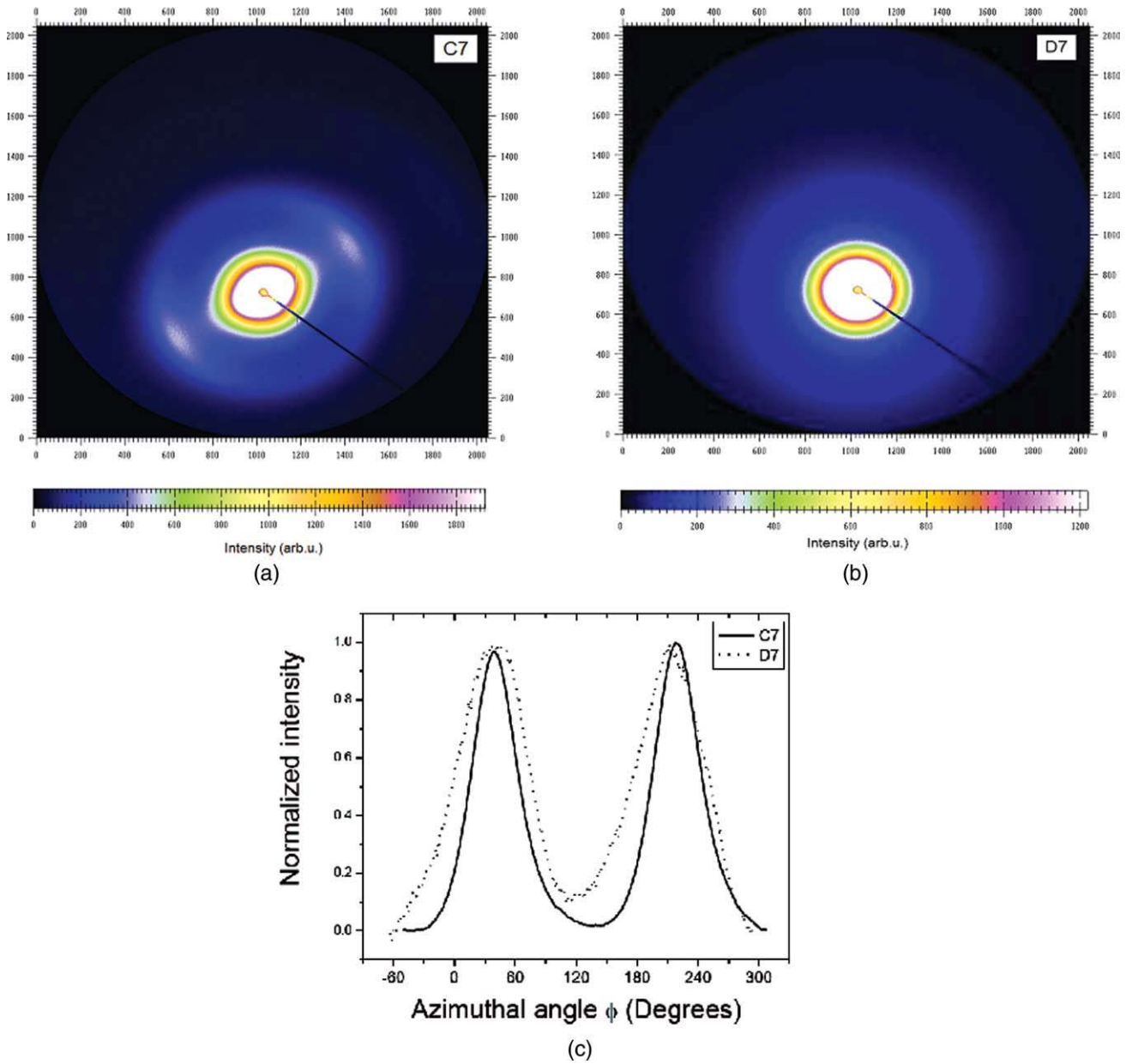


**Figure 2** 2D SAXS imagesof EVA/clay nanocomposites. (a) 7 wt % Cloisite®20A clay loading, $C_7$ sample (b) 7 wt % Cloisite®25A clay loading, $D_7$ sample. (c) azimuthal plot I(φ) versus φ for $C_7$ (solid line) and $D_7$ (doted line) nanocomposites. The data are averaged in the radial direction around the first reflection. [Color figure can be viewed in the online issue, which is available at wileyonlinelibrary.com.]

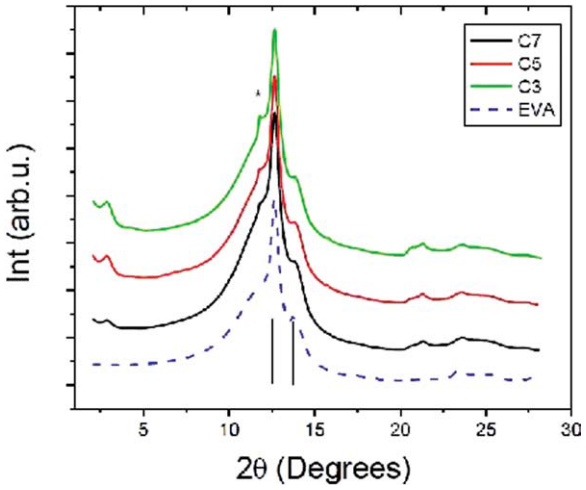


**Figure 3** Diffractograms for C series nanocomposites and neat EVA. The solid lines and the star indicate the peak positions from the principal diffraction lines of polyethylene and pristine clay structure, respectively. Dotted line for neat EVA. The curves are vertically shifted by an arbitrary scale factor. [Color figure can be viewed in the online issue, which is available at wileyonlinelibrary.com.]

polymeric matrix characteristics. Figure 3 shows the diffractograms for pure EVA sample and $C_3$, $C_5$, and $C_7$ nanocomposites. The low angle peaks observed for the nanocomposites (for $2\theta<5$) are related to polymer/clay intercalated structures and were already discussed in the previous paragraphs. The other features in the curves are mainly due to the crystalline and amorphous phases of the matrix. This is quite clear from the direct comparison with the pure EVA polymer diffractograms. The principal X-ray diffraction lines from polyethylene segments (PE), associated with interplanar distances of 4.11 and 3.71 Å can be identified whereas a small peak (indicated by a star in Fig. 3) with *d*-value equal to 4.42Å is due to the clay structure.

No significant changes in PE crystalline peak position or their integrated intensity are observed, showing that the effect of organoclays, Cloisite® 20A and 25A, on the crystalline phase and the degree of crystallinity of EVA is insignificant. Similar conclusions were pointed by Gelfer et al.,[23] suggesting that charged clay particles interact more favorably with polar amorphous vinyl acetate moieties, and hence, they are confined to the amorphous phase of the polymeric matrix.

## Scanning electron microscopy analysis

The SEM micrographs of pure clays Cloisite® 20A and 25A are shown in Figure 4(a,b) while the nanocomposites SEM images in Figure 4(c,h). From the images it can be seen that the surface morphology changes according to the clay loading.

Figures 4(c) and f show smooth surface indicating homogenous dispersion of organo clay in the polymer matrix. Figures 4 (d,e,g,h) show the micrographs of EVA/organoclay nanocomposites with increasing organoclay loading. These figures show rough surfaces and presence of some microscale fillers. As the filler loading increases, the formation of microfiller (agglomeration of individual silicate layers) is obtained because of the difficulties to achieve homogeneous dispersion. The agglomeration and the poor reinforcing effect of organoclay at higher loadings will result in deterioration of nanocomposite properties. The micrographs also show a better homogeneous dispersion of Cloisite® 25A organoclay in the EVA matrix for all the clay contents compared with Cloisite® 20A based nanocomposites.

## Transmission electron microscopy analysis

More information on the nanocomposites morphology was obtained by TEM analysis. Figure 5 shows the micrograph recorded for EVA filled with two different organoclays. The dark line shows the presence of silicates in the polymer matrix, whereas the bright area represents the polymer matrix. It shows the homogenous dispersion of individual silicate layers in the polymer matrix for low clay contents, but these stacks of layers lack a very good distribution within the polymer matrix at higher clay loadings resulting in the agglomeration of clay platelets. The distribution of the clay nanoplatelets in the EVA matrix appear to depend on the nature of the organomodified clay. Better results are observed for Cloisite® 25A series sample. The nanocomposite based on one bulky tail organoclay (Cloisite® 25A), exhibits a better dispersed morphology consisting primarily of individually dispersed clay platelets [see Fig. 5 (d,e)].

It follows that the EVA polymer chains must have an attractive energetic interaction with the pristine surface of the silicate. In fact, this notion is supported by the theoretical work of Tanaka and Goettler.[24] Two alkyl tails (as containing Cloisite® 20A) move the platelets much farther apart, thereby greatly reducing the cohesive forces between platelets; however, at the same time, these alkyls sterically diminish the opportunity for the polymer to interact with silicate surface and increase the amount of hydrocarbon that must unfavorably mix with the polymer in order for polymer-silicate contacts to be possible. The results show that this extreme leads to a nanocomposite structure having a low level of platelet exfoliation. On the other hand, the one-tail organic modifier, which leads to nearly complete organoclay dispersion in polymer apparently provides a good balance between platelet

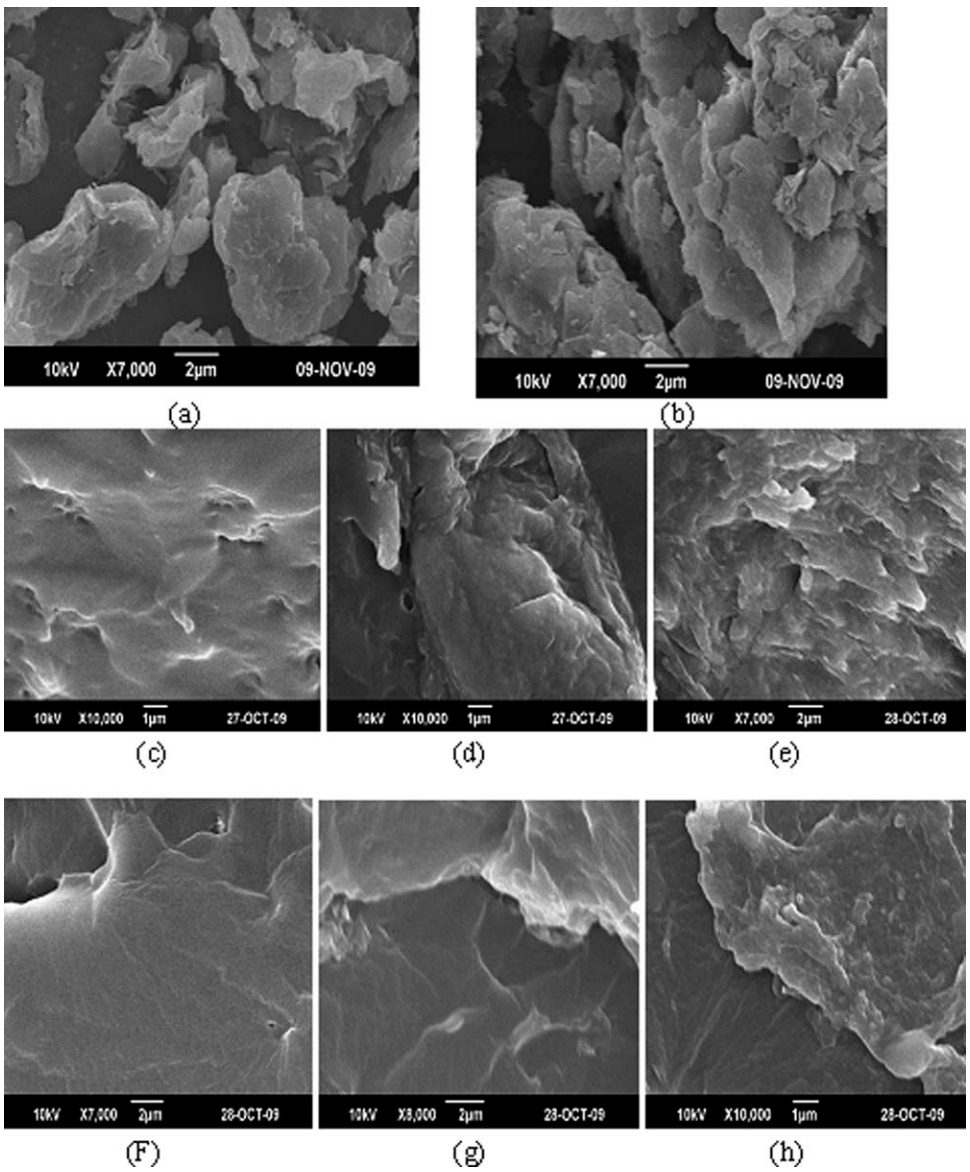


**Figure 4** SEM micrographs: (a) Cloisite® 20A nanoclay, (b) Cloisite® 25A nanoclay, (c) $C_3$, (d) $C_5$, (e) $C_7$, (f) $D_3$, (g) $D_5$, (h) $D_7$.

spacing, level of access to exposed silicate surface, and number of unfavorable interactions between the polymer and the alkyl units. In this case, the driving force for the polyamide to contact to the silicate surface is sufficiently greater than the penalty incurred by the mixing of polyamide chains and the alkyl units of the one-tail organic modifier. This is schematically represented in Figure 6.

### Positron annihilation life time spectroscopic analysis

Free volume sizes, fractions, and distributions in a variety of polymeric membranes have been reported using the PALS technique, which enables the detection of "voids" in polymers at an atomic scale.[25,26] For polymeric applications, *ortho*-positronium (*o*-Ps) lifetime and its probability of annihilation are related to the free-volume size and fraction, respectively. The positron annihilation lifetime of dense membranes were determined by detecting the prompt-rays (1.28 Me V) from the nuclear decay that accompanies the emission of a positron from the $^{22}$Na radioisotope and the subsequent annihilation-rays (0.511 MeV). The results of *o*-Ps lifetime is around 1–5 ns in polymeric materials.

The molecular transport through a polymeric membrane depends on the amount of existing free volume. The free volume is created by the inefficient chain packing of the polymer generated by the chain segments arrangement. The increase of the free volume facilitates diffusion process due to the creation

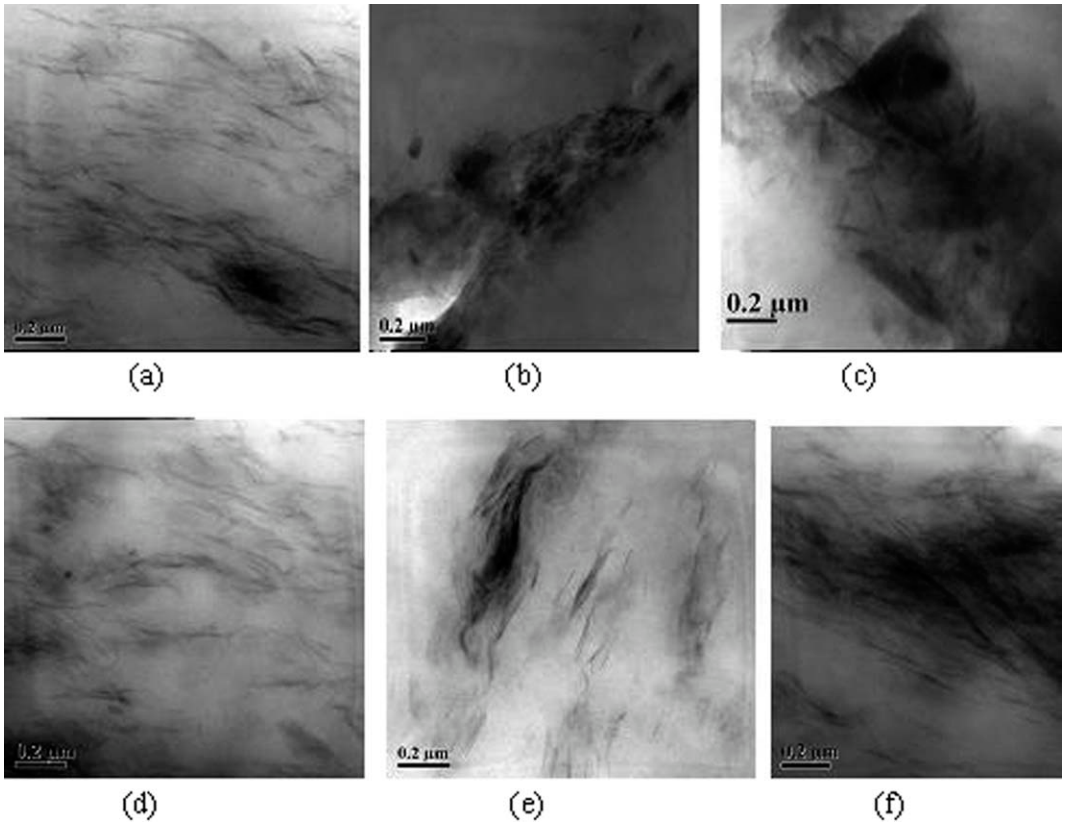


**Figure 5** TEM micrographs of EVA/organically modified clay nanocomposites. (a) 3 wt % Cloisite® 20A, (b) 5 wt % Cloisite® 20A, (c) 7 wt % Cloisite® 20A, (d) 3 wt % Cloisite® 25A, (e) 5 wt % Cloisite® 25A, (f) 7 wt % Cloisite® 25A.

of easier pathways for solutes. Positron Annihilation Lifetime Spectroscopy (PALS) is a non destructive technique that provides an effective approach for the study of the free volume in the solid state. It is based on the localization of the positronium (Ps) in the free volume holes because of their repulsion by the surrounding atoms. Generally, the annihilation spectra in polymers consist of three exponentially decaying components that correspond to the three main processes of their annihilation. Each of these processes is characterized by the mean life time and probability of annihilation (intensity). The longest life time corresponds to the annihilation process of *o*-Ps in the free volume holes. The size of free volume holes, R, in the polymer can be determined from the measured lifetime using semiempirical equation:

$$\left(\frac{1}{\tau_3}\right) = 2\left[1 - \left(\frac{R}{R_0}\right) + \left(\frac{1}{2\pi}\right)\sin\left(\frac{2\pi R}{R_0}\right)\right]. \quad (1)$$

Using this value of R, the free volume size ($V_f$) is calculated as $V_f = (4/3)\ R^3$. Then the relative fractional free volume is evaluated as the product of free volume ($V_f$) and *o*-$P_s$ intensity $I_3$. The effect of layered silicates on relative fractional free volume percentage is presented in Figure 7.

From the PALS data it is found that the relative fractional free volume of neat EVA decreases upon the addition of organoclay. The decrease is attributed to the interaction between layered silicates and polymer because of the platelet structure and high aspect ratio of the layered silicates. However, the free volume increases with increase in clay loading for both nanocomposites. The increase in the values can be attributed to the aggregation of fillers and the consequent additional void formation. It can also be deduced from the table that the relative fractional free volume percentage is lowest for D series samples. The decrease could be due to the better dispersion of organo modified layered silicates in the polymer matrix. It also could be explained due to the restricted mobility of the chain segments in the presence of layered silicates.

### Dielectric measurements

The formation of aggregates at higher filler loadings is also evident from the dielectric data shown in Figure 8. The dielectric loss for 3 wt % clay content was found to be minimum compared with higher loadings. The loss factor was found to be more for samples with higher clay loadings. Nonuniform distribution of the clay particles and the formation of larger

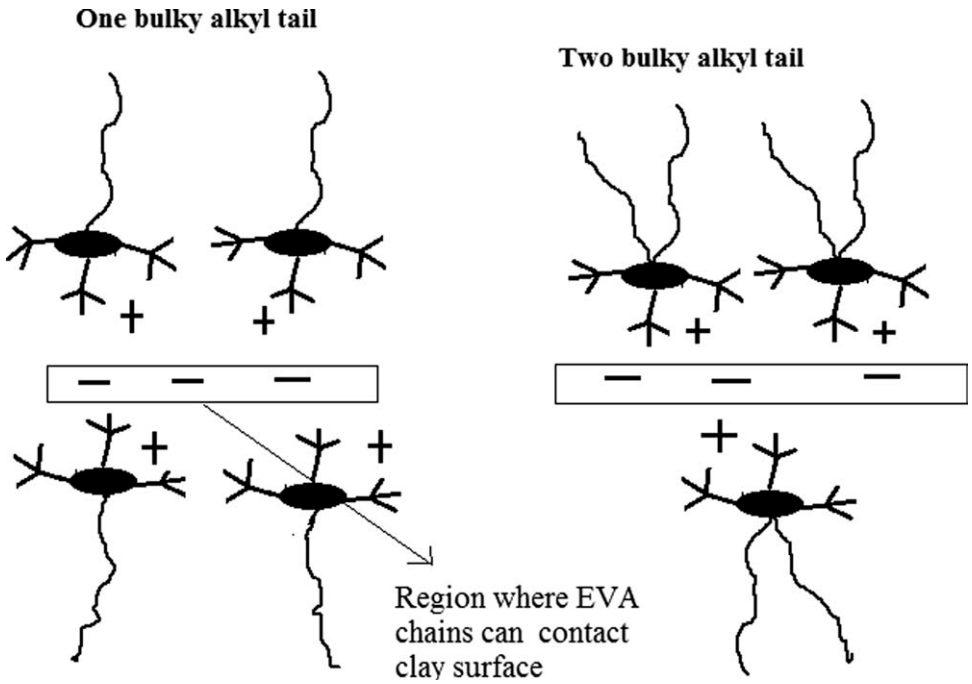


**Figure 6** Schematic illustration of the influence of bulky alkyl tails on dispersion of clay platelets in the polymer matrix.

clay aggregates in the matrix results in higher dielectric losses. Earlier research from our group also showed that dielectric loss values increases with higher clay loadings in EVA/non modified Montmorillonite nanocomposites.[27]

### Thermo gravimetric analysis

The thermogravimetric analysis (TGA) of the samples has been carried out to study the resistance of various nanocomposites toward thermal degradation. The results are reported in Figure 9. The thermo-oxidation of ethylene vinyl acetate copolymer (EVA) takes place in two steps. First, deacetylation is observed between 300 and 400°C, with production of gaseous acetic acid and formation of carbon–carbon double bonds along the polymer backbone. In a second step (between 400 and 500°C), the unsaturated chains are oxidized and volatilized. The first degradation of EVA/organo clay nanocomposites occurs at lower temperature than pure EVA because of the degradation of the organic modifier.[28] The presence of organic modifier and its degradation accelerates the degradation of acetic acid (This is the reason for maximum weight loss for composites at 400°C).

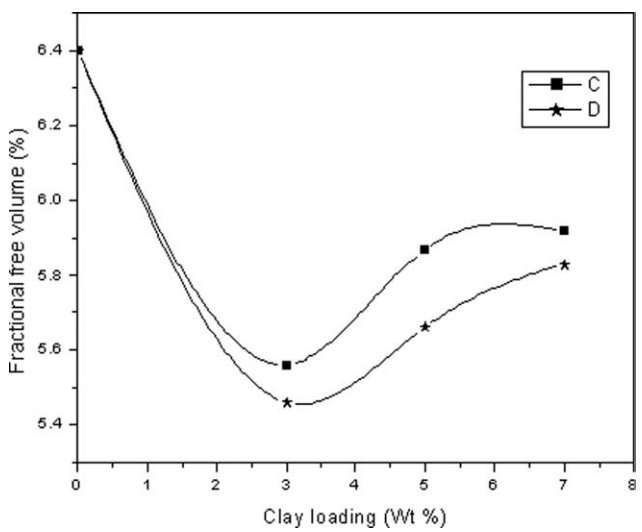


**Figure 7** Free volume as a function of nanoclay content.

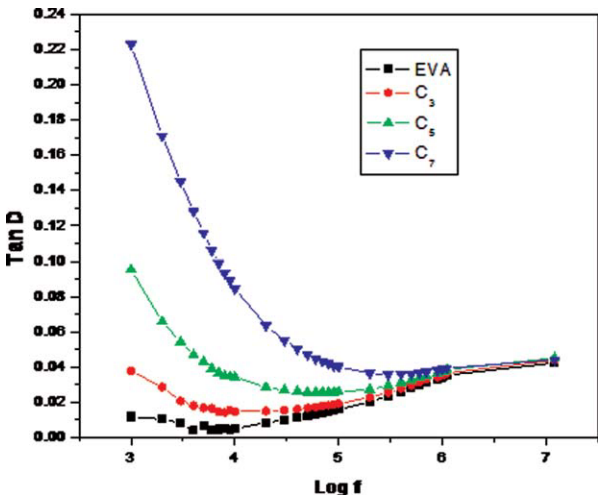


**Figure 8** Dielectric loss of EVA and C series of nanocomposites. [Color figure can be viewed in the online issue, which is available at wileyonlinelibrary.com.]

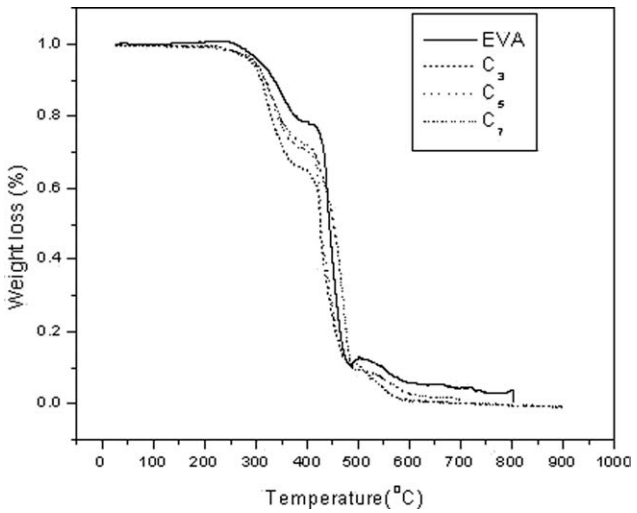


**Figure 9** TGA curves for pure EVA and C series of nanocomposites.

The second degradation of EVA/organo nanoclay composites filled with 3 phr of nanoclay occurs slightly at a higher temperature than pure EVA. The individual silicate nanolayers produce an effective shield to reduce the volatilization of the degradation product, and hence, the thermal stability of the material is increased. At higher organo clay loadings the thermal degradation is lower than pure EVA. This is mainly due to the agglomeration of clay platelets at higher loading.

### EVA/clay nanocomposite membrane for gas separation

The mass transport mechanism of gases permeating in a nanocomposite is similar to that in a semicrystalline polymer. The nanocomposite is considered to consist of a permeable phase where nonpermeable nano-platelets are dispersed. There are mainly three factors that influence the permeability of nanocomposites: the volume fraction of the nanoparticles, their relative orientation to the diffusion direction and their aspect ratio. The gas transport behavior of two different nanoclay reinforced EVA membranes has been analyzed using oxygen and nitrogen gases and the results were compared with neat EVA. Oxygen permeability is shown in Figure 10. EVA/clay nanocomposites exhibit excellent barrier properties. The decreased permeability of the nano composites arises from the longer diffusion pathway that the penetrants must travel in the presence of clay nanolayers. In general, there are two reasons for the enhancement of gas barrier property in polymer/clay nanocomposites. First, gas impermeable nanoclay layers dispersed in the polymer matrix form tortuous path way, which retard the diffusion of the gas molecules through the composites. Second, exfoliated and intercalated clay layer bundles strongly restrict the motions of polymer chain probably reducing the coefficient of diffusion of the gas molecules.

A decrease of the solubility is expected in nanocomposite due to the reduced polymer matrix volume, as well as a decrease in diffusion due to a more tortuous path for the diffusing molecules. The reduction of the diffusion coefficient is higher than that of the solubility coefficient. Indeed, the volume fraction of nanoplatelets is low and, thus, the reduction of the matrix volume is small. The major factor, then, is the tortuosity, which is connected directly to the shape and the degree of dispersion of nanoplatelets.

It is found that Cloisite® 25A reinforced EVA composites showed better gas barrier properties than Cloisite® 20A. The main factors that affect the permeation properties of two nanocomposites in different way are the degree of dispersion and the aggregation of the silicate layers. Better dispersed clay systems increase the tortuosity path of the diffusing molecules where as larger aggregates decrease the aspect ratio of the nanoparticles and can act as a low resistance pathway for the gas transport.

The influence of clay loading on permeability can easily be noticed in Figure 10. The permeability increases as a function of clay loading. This result is in close correlation to microscopic and PALS results. SEM and TEM images show agglomeration of clay particles at higher clay loading. PALS measurements show that fractional free volume percentage increases with clay loading. Hence, these samples showed reduced barrier properties.

The effect of penetrant size on the diffusion of gas molecules through nanocomposites membranes can

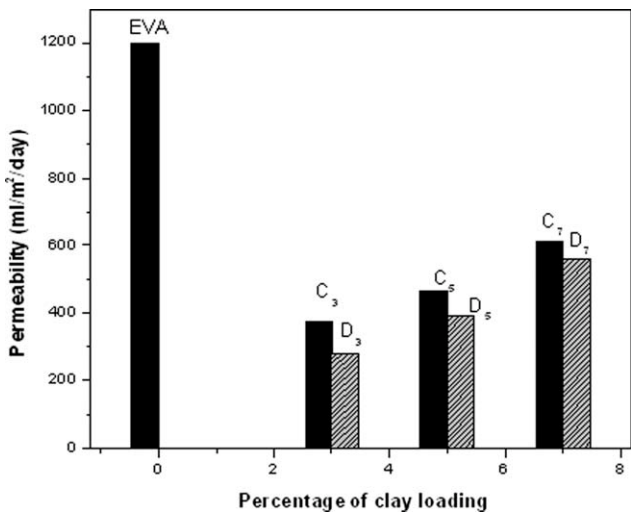


**Figure 10** Permeability of Oxygen gas through EVA/clay nanocomposites.

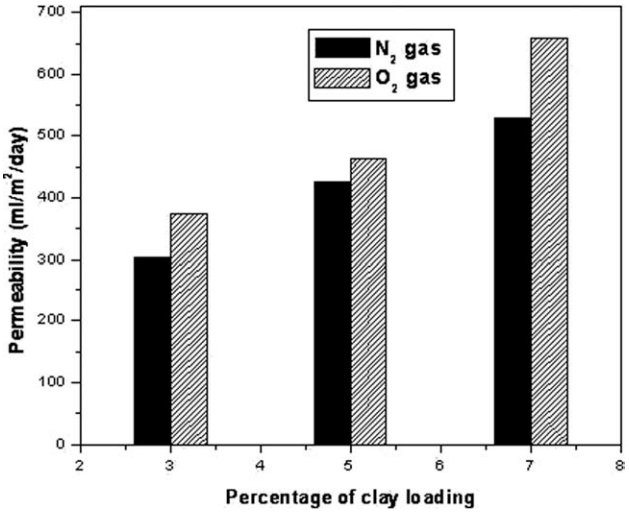


**Figure 11** Nitrogen and Oxygen gas permeability through C series of samples.

be understood from the permeation properties presented in Figure 11. It is found that oxygen has more permeability than nitrogen for samples with same clay content. This is due to the difference in the kinetic diameter of the gases. The kinetic diameter of nitrogen and oxygen are found to be 3.64 Å and 3.46 Å units, respectively. Since oxygen has got the lowest kinetic diameter it can easily pass through the matrix. Hence, these modified membranes are more selective towards oxygen.

### Permeation models

Nielsen model has been applied to predict the dependence of gas permeability on the filler volume fraction.[29] This model introduced the basic concept of tortuosity factor to predict the effective permeability as a function of the clay volume

$$\frac{P}{P_0} = \frac{1-\theta}{1+(\alpha/2)\theta}, \tag{2}$$

Where $P$ and $P_0$ are the permeabilities of the composite and that of neat polymer, respectively, $\theta$ is the volume fraction of the filler and $\alpha$ is the aspect ratio. Lan et al.[30] estimated the aspect ratios of the fillers in polyimide/clay nanocomposites. Furthermore, quite recently a review has been addressed by Choudalakis and Gotsis[1] in which authors emphasis various models that have been proposed for the prediction of the permeability in nanocomposites. The experimental data were fitted using Nielson equation and the aspect ratio falls in between 26 and 115.

In Nielson model, the dependence of permeability on the relative orientation and state of dispersion of the clay platelets is not taken into consideration. The tortuosity factor expression can be modified including the orientational order S as indicated by Bharadwaj.[31] Then the relative permeability is given by:

$$\frac{P_s}{P_p} = \frac{1-\theta_S}{1+\frac{L}{2W}\theta_S\left(\frac{2}{3}\right)\left(S+\frac{1}{2}\right)}, \tag{3}$$

The above expression reduces to eq. (2) when $S = 1$ (plannar arrangement of the clay platelets) and converges approximately to the permeability of the pure polymer when $S = -1/2$ (orthogonal arrangement). The barrier property is enhanced when $S = 1$ and decays in a continuous fashion as predicted in eq. (3) nearly that of the pure polymer when $S = -1/2$, where the sheets are supposed to be arranged such that there is negligible decrease in the tortuosity. The various orientations of the silicate layers in the polymeric matrix are schematically represented in the Figure 12.

Experimental data of relative permeability were analyzed using eq. (3). Considering random particle orientation ($S = 0$), the calculated aspect ratio was found to be 233 for D samples. It is interesting to note that the calculated aspect ratio is much higher than that obtained from Nielsen model [eq. (2)]. The experimental permeability values of D samples and the calculated values using the Bharadwaj's model are presented in Figure 13. The results are in line with the prediction expected from Bharadwaj's model at lower concentration of clay but, at higher concentration of clay contents, the experimental data deviates from calculated curve. This is mainly due

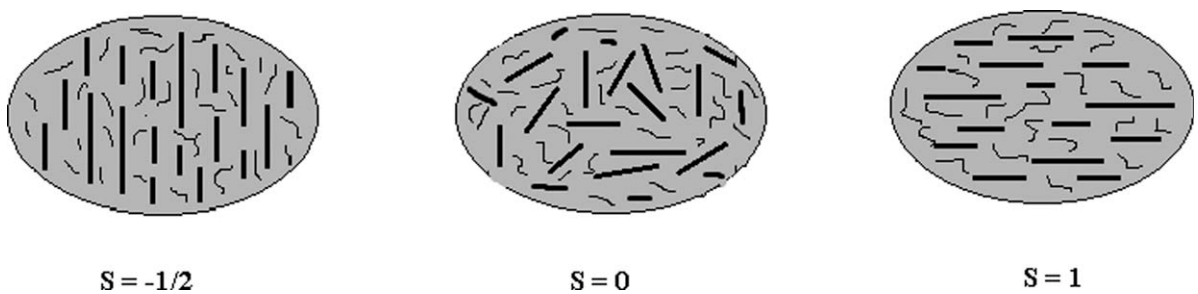


**Figure 12** Illustrations showing the dependence of the orientational parameter S as a function of the preferred orientation of clay platelets (thick dark lines).

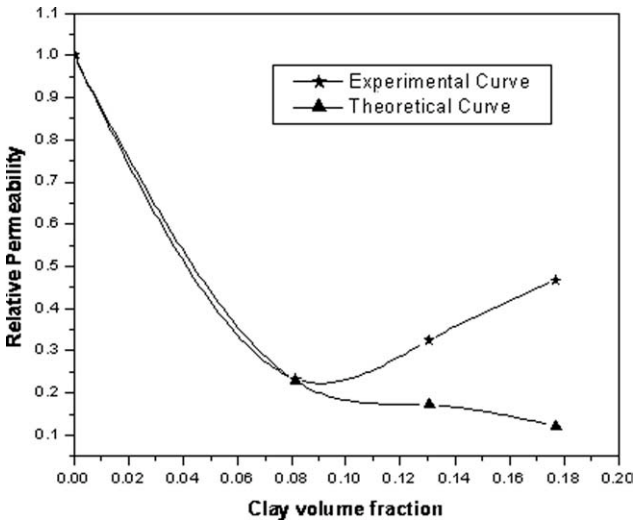


**Figure 13** Relative Oxygen permeability as a function of clay volume fractions. Experimental values and calculated curve using Bharadwaj model [eq. (3)].

to the agglomeration of clay platelets at higher clay loadings. Agglomeration results in increased free volume and hence the permeability increases.

## CONCLUSIONS

EVA/clay nanocomposites with two different organomodified clays (Cloisite® 20A and 25A) were prepared and their barrier features were compared. The morphology of the composites was analyzed by X-ray scattering, SEM and TEM. The SAXS results showed similar degree of polymer intercalation between the silicate layers in both kind of organoclays but a better dispersion of the layers and more homogeneous films are obtained for Cloisite® 25A based nanocomposites. WAXS measurement confirmed that the addition of clay platelets did not modify the crystalline structure or the degree of crystallinity of the polymeric matrix. SEM and TEM also showed better homogeneous dispersion of clay platelets for the nanocomposite of samples with Cloisite® 25A. The dispersion of nanoparticles seems to be maximized for 3 wt % of clay and agglomeration increases for higher clay loading. This observation was also confirmed by the dielectric loss measurements. The fractional free volume of the polymer has a minimum value upon the addition of 3 weight percentage of filler but increases at higher clay concentrations. The membranes based on Cloisite® 25A exhibited lower permeability to oxygen and nitrogen gases compared with the other organoclay due to enhanced polymer-filler interaction. Hence, it is important to mention that due to the incorporation of organo modified clay into EVA; highly selective barrier membranes could be developed. Finally, different models have been applied to explain the observed permeability of nanocomposites. The results are in line with the prediction by Bharadwaj model at lower concentration of clay but at higher concentration of clay, the experimental values deviates from expected values.

SAXS and WAXS data were collected at the I711 and 911-5 beamlines, respectively, of the MAX-lab synchrotron facility using beamtime granted to TSP.

## References

1. Choudalakis, G.; Gotsis, A. D. Eur Polym Mater 2009, 45, 967.
2. Schmidt, D.; Shah, D.; Giannelis, E. P. Curr Opin Solid State Mater Sci 2002, 6, 205.
3. Pinnavaia, T. J.; Beall, G. W. Polymer-Clay Nanocomposites; John Wiley and Sons: New York, 2000.
4. Beyer, G. Plast Additives Compound 2002, 4, 22.
5. Zheng, X.; Wilkie, C. A. Polym Degrad Stab 2003, 81, 539.
6. Iyer, P.; Iyer, G.; Coleman, M. J Membr Sci 2010, 358, 26.
7. Ahn, J.; Chung, W. J.; Pinnau, I.; Song, J.; Du, N; Robertson, G. P.; Guiver, M. D. J Membr Sci 2010, 346, 280.
8. Chavarria, F.; Paul, D. R. Polymer 2006, 47, 7760.
9. Madaleno, L.; Schjodt-Thomsen, J.; Pinto, J. C. Compos Sci Tech 2010, 70, 804.
10. Anil kumar, S.; Yuelong, H.; Yumei, D.; Le, Y.; Kumaran, M. G.; Thomas, S. Ind Eng Chem Res 2008, 47, 4898.
11. Guo, Z.; Lee, L. J.; Tomasko, D. L. Ind Eng Chem Res 2008, 47, 9636.
12. Maji, P. K.; Das, N. K.; Bhowmick, A. K. Polymer 2010, 51, 1100.
13. Adame, D.; Beall, G. W. Appl Clay Sci 2009, 42, 545.
14. Madhavan, K.; Reddy, B. S. R. J Membr Sci 2009, 342, 291.
15. Khounlavong, L.; Ganesan, V. J Chem Phys 130: 104901 2009.
16. Knaapila, M.; Svensson, C.; Barauskas, J.; Zackrisson, M.; Nielsen, S. S.; Toft, K. N.; Vestergaard, B.; Arleth, L.; Olsson, U.; Pedersen, J. S.; Cerenius, Y. J Synchrotron Rad 2009, 16, 498.
17. Hammersley, A. P.; Svensson, S. O.; Thompson, A.; Graafsma, H.; Kvick, E.; Moy, J. P. Rev Sci Instrument 1995, 66, 2729.
18. Koo, C. M.; Kim, S. O.; Chung, I. J. Macromolecules 2003, 36, 2748.
19. Mammen, C. B.; Ursby, T.; Cerenius.Y.; Thunnissen, M.; Als-Nielsen, J.; Liljas, A. L. Acta Physica Polonica A 2002, 101, 595.
20. Gelfer, M.; Song, H. H.; Liu, L.; Avila-Orta, C.; Yang, L.; Si, M.; Hsaio, B. S.; Chu, B.; Rafailovich, M.; Tsou, A. H. Polym Eng Sci 2002, 42, 1841.
21. Vaia, R. A.; Giannelis, E. P. Macromolecules 1997, 30, 7990.
22. Vaia, R. A.; Giannelis, E. P. Macromolecules 1997, 30, 8000.
23. Gelfer, M.; Burger, C.; Faddev, A.; Scis, I.; Chu, B.; Hsaio, B. S.; Henitz, A.; Kojo, K.; Hsu, S-L.; Si, M.; Rafailovich, M. Langmuir 2004, 20, 3746.
24. Tanaka, G.; Goettler, L. A. Polymer 2002, 43, 541.
25. Jean, Y. C.; Mallon, P. E.; Zhang, R.; Chen, H.; Li, Y.; Zhang, J.; Wu, Y. C.; Sandereczki, T. C.; Suzuki, R.; Ohdaria, T.; Gu, X.; Nguyen, T. Rad Phys Chem 2003, 68, 395.
26. Zhang, J.; Chen, H.; Li, Y.; Suzuki, R.; Ohdaria, T.; Jean, Y. C. Rad PhysChem 2007, 76, 172.
27. Muralidharan, M. N.; Anil Kumar, S.; Thomas, S. J Membr Sci 2008, 315, 147.
28. Ardhyananta, H.; Ismail, H.; Takeichi, T. J. Reinf Plast Comps 2007, 26, 789.
29. Van Amerongen, G. J. J Polym Sci 1950, 5, 307.
30. Lan, T.; Kaviratna, P. D.; Pinnavaia, T. J Chem Mater 1994, 6, 573.
31. Bharadwaj, R. K. Macromolecules 1989 2001, 34.